Journal of Energy and Power Engineering 9 (2015) 1047-1055
doi: 10.17265/1934-8975/2015.12.002

Numerical Simulation of $Cu(In,Ga)Se_2$ Solar Cells Performances

Daouda Oubda[1, 2], Marcel Bawindsom Kebre[1], François Zougmoré[1], Donatien Njomo[2] and Frédéric Ouattara[1, 3]

1. LA.M.E (Laboratoire de Matériaux et Environnement), UFR-SEA (Unité de Formation et de Recherche en Sciences Exactes et Appliquées), Université de Ouagadougou, Ouaga 03 BP 7021, Burkina Faso

2. L.A.T.E.E (Laboratoire d'Analyse des Technologies de l'Energie et de l'Environnement)—FAST (Faculté des Sciences et Techniques)-Sciences, Université Yaoundé I, Yaoundé 812, Cameroun

3. LA.R.E.M.E (Laboratoire de Recherche en Energétique et Météorologie de l'Espace), ENS (Ecole Normale Supérieure), Université de Koudougou, Koudougou BP 376, Burkina Faso

Received: August 27, 2015 / Accepted: September 29, 2015 / Published: December 31, 2015.

Abstract: This paper presents a numerical characterization of copper-indium-gallium-diselenide thin film solar cells using one dimensional simulation program (SCAPS-1D). We have performed an optimization of the performances of the standard Mo/Cu(In,Ga)Se_2/CdS/ZnO solar cells using current-voltage and quantum efficiency methods. With a $CuIn_{0.7}Ga_{0.3}Se_2$ absorber, we have investigated the buffer layer thickness, temperature, series and shunt resistances effects on the open-circuit voltage, short-circuit current density, fill factor, conversion efficiency and quantum efficiency. The simulated results show good performances when the thickness of the buffer layer is in the range of 10-40 nm due to the reduction of absorption in the short wavelenghts (380-500 nm). High performances of the model is obtained when the series and shunt resistances is in the range of 0.1-1 Ω·cm² and 1,000 Ω·cm², respectively. Under these conditions, the cell can theoretically operate under an ambiant temperature of 370 K without any loss of its performances.

Key words: Numerical simulation, SCAPS-1D, CdS thickness, temperature, R_S, R_{sh}.

1. Introduction

The current challenge in the photovoltaïque area is low cost, high conversion efficiency, good stability, mass production and accessibility for all.

Copper-indium-gallium-diselenide CIGS ($Cu(In_{1-x}Ga_x)Se_2$) films are considered as the most promising materials for achieving the goals of low-cost and high performance solar cells [1]. The best CIGS thin-film solar cell has reached a conversion efficiency of 20.8% [2]. In addition to this high efficiency, it is possible to increase the stability and the performances of the device through the optimization of layers properties.

The main advantage of CIGS solar cell comes from the high direct band gap of the absorber and the window layers (respectively 1.2 eV and 3.3 eV). Furthermore, there is the possibility of adding a buffer layer between these layers.

Theoretically, the solar cell using ZnO as buffer layer provided a good performance [3], but the sputter deposition method use for this layer is a serious problem, because in practice, it can damage the absorber layer. A thin film buffer layer of cadmium sulfide (CdS) is necessary to protect the absorber layer. It also points out that, the diffusion of cadmium in the absorber provides positive effects [1, 4]. The presence of the buffer layer is expected to reduce interface and bulk recombination and ameliorate the performances of the cell [5]. Generally, other parameters such as temperature, series (R_S) and shunt (R_{Sh}) resistances are

Corresponding author: Daouda Oubda, doctorant, research field: CIGS solar cells characterization.

also factors limiting the performance of CIGS solar cells. It is very important to propose a theoretical model where the effects of these parameters are optimized.

Analytical and numerical approaches are generally used to analyze the influence of the CIGS absorber and hetero-interface as limiting factors of the conversion efficiency [6].

Numerical characterization of (CIGS) solar cells is an effective tool for understanding and solving very complex phenomena, it permits to increase the efficiency of conversion and the stability.

The computer simulation tool SCAPS-1D (a solar cell capacitance simulator in one dimension) has been developed to simulate the electrical characteristics, direct current (dc) and alternating current (ac) of cadmium telluride (CdTe) and CIGS solar cells [3, 7, 8]. SCAPS-1D permits to characterize solar cells through current-voltage (*J-V*) and quantum efficiency (*QE*). *J-V* and *QE* characteristics permit to detect the losses of current by reflection, incomplete collection and recombination in the different layers and are useful to optimize cells performances [9].

In this paper, we characterize Mo/Cu(In,Ga)Se$_2$/CdS/ZnO solar cells through *J-V* characteristics and quantum efficiency *QE* (λ). We are interested in the effects of the buffer layer thickness, temperature, series and shunt resistances on the energetic and electrical performances of the solar cell.

2. Materials and Methods

2.1 CIGS Solar Cells Structure

Fig. 1 below presents our solar cells model structure.

It is constituted by four semi-conductor layers and two metallic contact layers. Among the semi-conductor layers, we have the substrate which is the support of the device. It has been found that, the diffusion of sodium coming from the substrate in the CIGS absorber improves the performances of the solar cells [10, 11]. The effects of sodium is to enhance the solar cell efficiency mainly due to higher open circuit voltage (V_{OC}) and fill factor (*FF*) by increasing hole

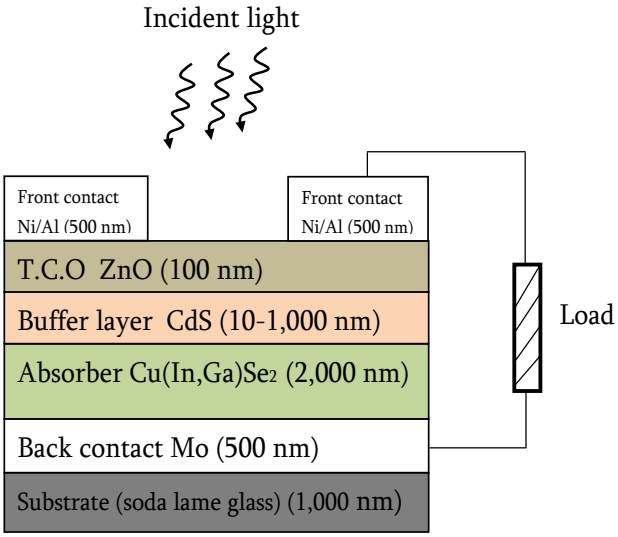

Fig. 1 Schematic structure of typical CIGS solar cells.

density and film conductivity [12]. With a direct band gap of 1.2 eV, the absorber layer is the most important element of the solar device. This band gap energy is near the ideal value for the sunlight spectrum absorption which is situated at 1.4 eV [10] and used in high efficiency CIGS solar cells conception. It is a *p*-type conductivity layer inside which photons are converted to electron-hole pairs.

We use cadmium sulfide as buffer layer, it is a *n*-type conductivity and direct band gap of 2.4 eV. The Cd diffuses into the CIS (copper-indium-selenide) layer, resulting in a *n*-type region, and this Cd doping may play an important role in the formation of a *p-n* junction inside the absorber layer [4]. The CdS layer is followed by the deposition of T.C.O (transparent conductive oxide) ZnO [13]. Its high direct band gap of 3.3 eV allows a large number of photons to reach the absorber layer. Between the substrate and absorber, we have a molybdenum layer. It represents the back contact and is useful for holes collection. Finally, we have the front contact which collects electrons and is constituted by nickel/aluminum.

2.2 Numerical Simulation

Numerical simulation is an important tool for the characterization of solar cells. It has the advantage to control all device and material properties. They enable

us to do input parameters of the model and quantify changes in current-voltage (*J-V*) or quantum efficiency (*QE* (λ)) trends [9]. Several software, among which SCAPS-1D, ASA (analysis of silicon amorphous), PC-1D (photonic computer one dimension), AFORS-HET (program for simulation of heterojunction solar cell) and AMPS-1D (analysis of microelectronic and photonic structures one-dimension), have been developed in order to simulate the functioning of solar cells [14]. SCAP-1D is widely used for the simulation of CIGS and CdTe based solar cells.

The good agreements between SCAPS-1D simulation results and the existing experimental ones motivated us to use this tool in our work [14].

SCAPS calculates solution of the basic semi-conductor equations in one dimensional and in steady state conditions [15]. These are Poison's equation for electrostatic potential φ , and the continuity equations for electrons and holes with the approximate boundary conditions [15, 16].

Poison's equation used for semi-conductor is [9]:

$$\nabla \cdot \varepsilon \nabla \varphi = -q\left(p - n + N_D^+ - N_A^-\right) \quad (1)$$

The continuity equations for electrons and holes are, respectively:

$$\nabla \cdot \vec{J}_n = q(R - G) + q\,\partial n/\partial t \quad (2)$$

$$\nabla \cdot \vec{J}_p = -q(R - G) + q\,\partial p/\partial t \quad (3)$$

where, ε is the dielectric constant, φ is the electrostatic potential, n and p are, respectively the free carrier concentrations for electron and hole, N_D^+ and N_A^- are the density of ionized donor and acceptor, J_n and J_p are electron and hole current density, R is the recombination rate and G is the generation rate.

In a case of stationary conditions, we have:

$$\partial n/\partial t = \partial p/\partial t = 0 \quad (4)$$

Eqs. (2) and (3) become:

$$\nabla \cdot \vec{J}_n = q(R - G) \quad (5)$$

$$\nabla \cdot \vec{J}_p = -q(R - G) \quad (6)$$

The recombination term in Eqs. (5) and (6) has non-linear dependencies on the carrier concentrations n and p, the resolution method is given in Ref. [9]. All simulations use Fermi-Dirac statistics given by Eq. (7) [9]:

$$f(E) = 1/\left(1 + \exp\left[\left(E - E_f\right)/kT\right]\right) \quad (7)$$

where, E is the energy level of particle, E_f is the equilibrium Fermi level energy, k is the Boltzmann constant and T is the absolute temperature.

Table 1 [1, 15, 17-21] summarizes the parameters of the different layers used in this paper in accordance with Fig. 1. All simulation has been performed under an AM.1.5 solar light spectrum with an incident power density 100 mW/cm².

3. Results and Discussion

3.1 Comparison with Experimental Data

Fig. 2 below showed a superposition of *J-V* and *QE* (λ) curves of experimental data [19] and the simulated CIGS solar cells for our baseline.

The resulting performance parameters of the open circuit voltage (V_{OC}), short circuit current density (J_{SC}), fill factor (*FF*), and efficiency (η) are determined using *J-V* characteristics and are shown in Table 2.

We notice that, the experimental J_{SC} is slightly higher than the simulated one and V_{OC} more lowly, nevertheless an excellent agreement was observed. In contrast, the quantum efficiency curves show a slight difference in the two configurations (experimental and simulated).

3.2 Effects of the Buffer Layer Thickness

Fig. 3 presents *J-V* characteristics and quantum efficiency as a function of the CdS thickness at 300 K. Table 3 shows the electrical parameters extracted from the *J-V* characteristics.

The open circuit voltage of device varies slightly with the increase of the CdS layer thickness, but the short circuit current density decreases considerably, particularly for large thickness (Fig. 3a).

Table 1 Base parameters of CIGS cell properties. Φ_b—barrier height ($\Phi_{bn} = E_C - E_F$, $\Phi_{bp} = E_F - E_V$), S—surface recombination velocity, W—layer width, ε—dielectric constant, μ—mobility, Doping (electron/hole density), E_g—band gap energy, N_C and N_V—effective density of states, ΔE_C—conduction band offset, N_{AG}—acceptor-like defect density, N_{DG}—donor-like defect density, E_A, E_D—peak energy in, σ_e, σ_h—capture cross section electrons and holes, χ_e—electron affinity, υ—thermal velocity, W_G—characteristic energy, N_a, N_d—shallow uniform acceptor and donor density.

	Contacts properties right	Left
Φ_b (eV)	$\Phi_{bn} = 0.0$	$\Phi_{bp} = 0.15$
S_e (cm/s)	10^7	10^7
S_h (cm/s)	10^7	10^7
Reflectivity	0.05	0.8

	Layers properties *p*-CIGS	*n*-CdS	*n*-ZnO
W (nm)	2×10^3	-	10^2
E_g (eV)	1.2	2.4	3.3
χ_e (eV)	4.5	4.15	4.45
$\varepsilon/\varepsilon_0$	13.6	10	9
N_c (cm^{-3})	2.2×10^{18}	2.2×10^{18}	2.2×10^{18}
N_v (cm^{-3})	1.8×10^{19}	1.8×10^{19}	1.8×10^{19}
υ_e (cm/s)	10^7	10^7	10^7
υ_h (cm/s)	10^7	10^7	10^7
μ_e (cm²/Vs)	10^2	10^2	10^2
μ_h (cm²/Vs)	25	25	25
N_a (cm^{-3})	7×10^{15}	-	-
N_d (cm^{-3})	-	2×10^{17}	10^{18}
ΔE_C (eV)	0.35	-0.3	
	Bulk defect properties *p*-CIGS	*n*-CdS	*n*-ZnO
σ_e (cm²)	6.1×10^{-14}	10^{-17}	10^{-14}
σ_h (cm²)	10^{-14}	10^{-13}	10^{-15}
N_{AG}, N_{DG} (cm^{-3})	3×10^{14} (d)	10^{17} (a)	10^{13} (a)
E_A, E_D (eV)	0.6	1.2	1.65
W_G (eV)	0.1	0.1	0.1

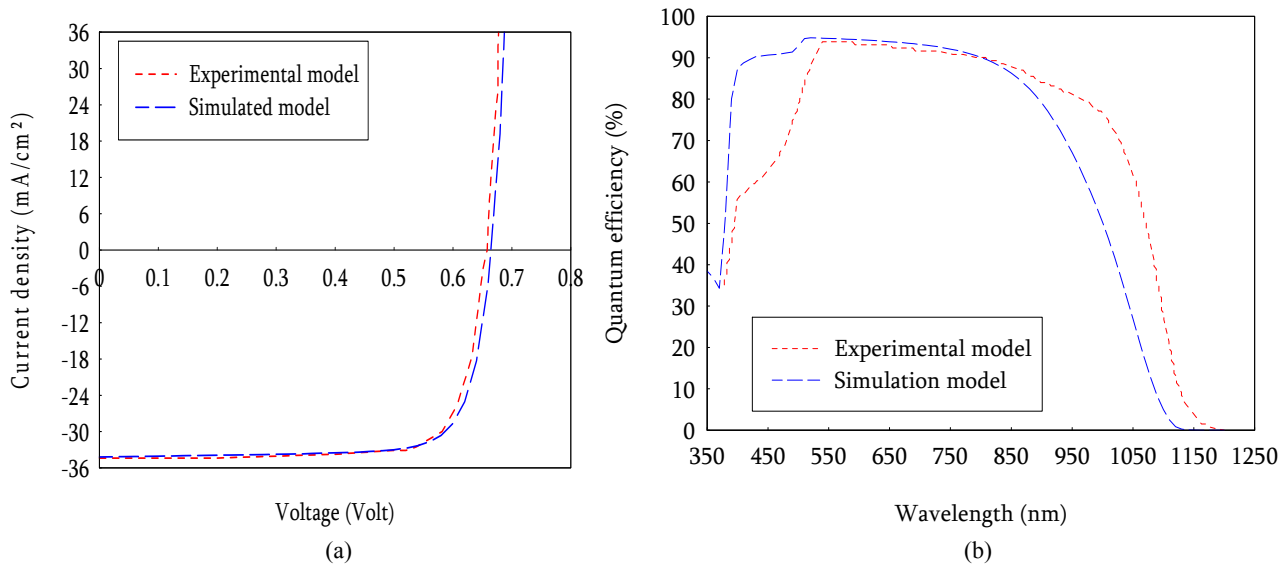

(a) (b)

Fig. 2 Simulated and experimental curves of (a) *J-V* characteristics and (b) quantum efficiency.

Table 2 Electrical parameters of experimental and simulated model.

	V_{OC} (V)	J_{SC} (mA/cm²)	FF (%)	η (%)
Experimental	0.64	34.6	79.5	17.7
simulated	0.6653	34.197	78.25	17.8

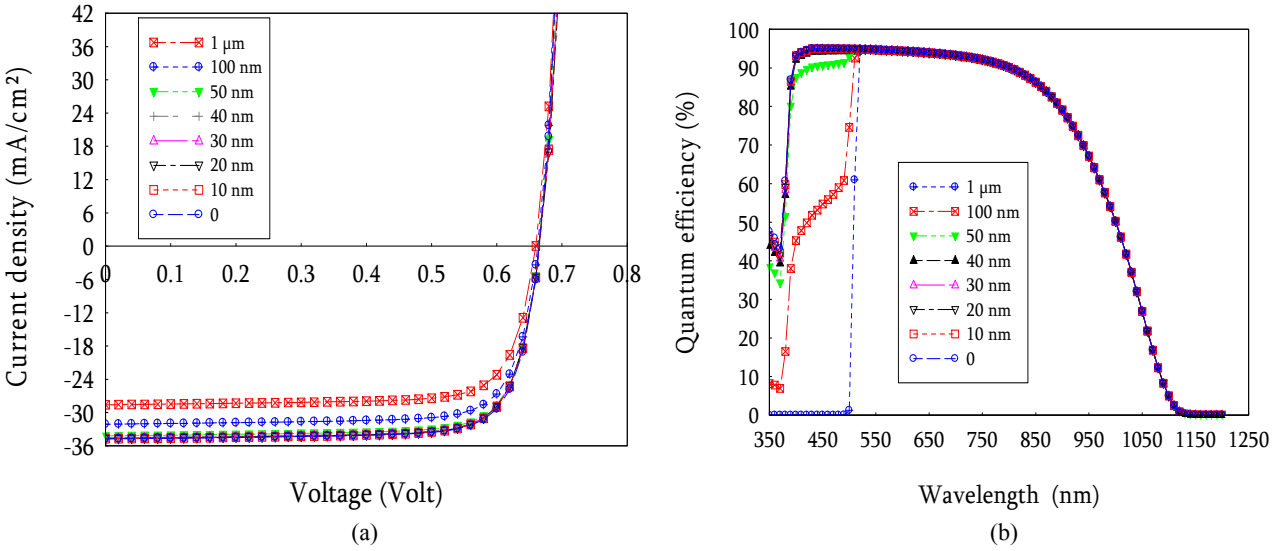

(a) (b)

Fig. 3 (a) *J-V* characteristics, (b) quantum efficiency as a function of CdS thickness.

This can be explained by the quantity of photons that, reach the absorber layer should decrease due to the increase of the absorption in the CdS layer (Fig. 3b). Fig. 3b effectively shows that, when the thickness of CdS exceeds 50 nm, the absorption in the CdS layers increase. In addition, the electron-hole pairs proceeded from these absorbed photons recombine in the CdS bulk for large thickness and do not collect. The effects of the buffer layer thickness on the electrical parameters have been also reported by Chelvanathan, et al. [3]. On the other hand, these results can be explained by an increasing of series resistance in the cell proportionally to the thickness of CdS. Eisenbarth, et al. [22] have also found that, the current through the devices is limited by a significant series resistance caused by the bulk resistivity of the CdS, which increases with increasing CdS thickness.

Table 3 below confirms that, the values of J_{SC} decrease considerably, but the decrease of V_{OC} is not significant has showed in Fig. 3b. In addition, we notice in Table 3, an important decrease of the conversion efficiency which is a direct consequence of J_{SC} and V_{OC} losses.

A thin buffer layer of 10-40 nm thickness is good to obtain a high performance and stability solar cells.

3.3 Effects of Operating Temperature

In this section, the effect of the operating temperature on *J-V* characteristics and *QE* (λ) is described. Fig. 4 presents the *J-V* characteristics and the quantum efficiency of CIGS solar cells using 30 nm of CdS buffer layer for different temperature.

Temperature is a limiting factor of the solar cell performances. The present work shows that, the current voltage characteristic is severely affected by the operating temperature, in particular the open circuit voltage. From different *J-V* curves (Fig. 4a), we observe a decrease of the open circuit voltage when increasing the temperature.

At high temperature, parameters such as the electrons and holes mobility, carrier concentrations and band gaps of the materials would be affected, which leads to a lower conversion efficiency [3].

Table 3 Electrical parameters as a function of CdS thickness at 300 K.

e (μm)	V_{OC} (V)	J_{SC} (mA/cm²)	η (%)
0	0.6657	34.746	18.16
10	0.6659	34.711	18.06
20	0.6659	34.692	18.03
30	0.6658	34.662	18.01
40	0.6657	34.546	17.99
50	0.6657	34.196	17.8
100	0.6634	32.08	16.63
1,000	0.6599	28.59	14.66

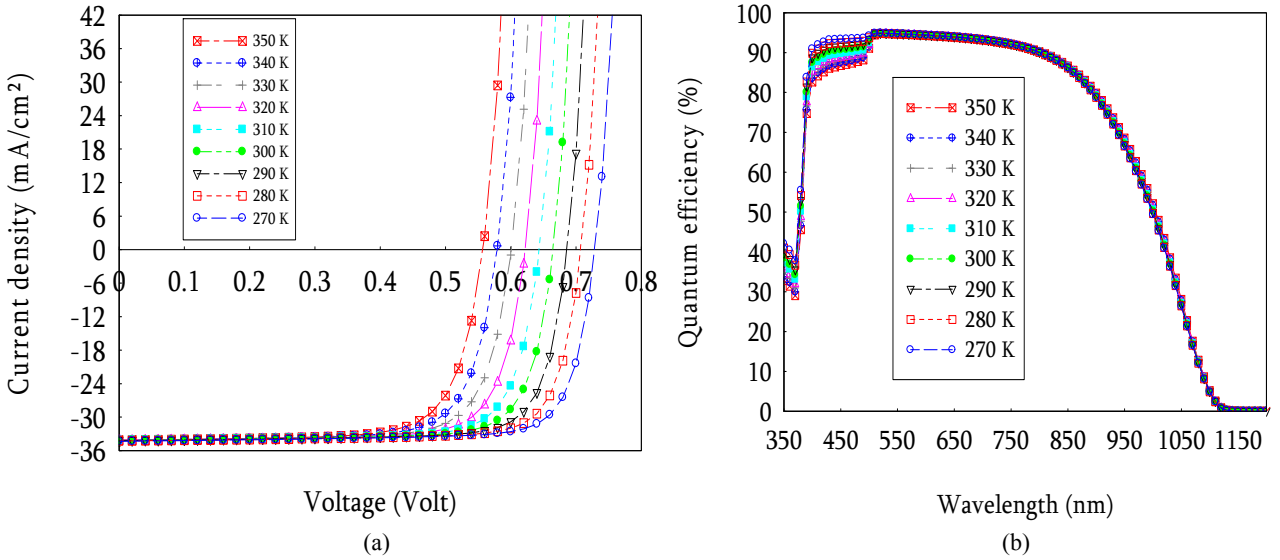

(a) (b)

Fig. 4 (a) *J-V*, (b) *QE* (λ) curves as a function of operating temperature.

This can be explained by majority charge carriers recombination in the space charge region and at CIGS/CdS interface before reaching the metallic contacts. As shown in Table 4 and highlight in Fig. 4b, the trend of the short circuit current density does not depend of the temperature. This is due to the fact that, the generation process $G(x)$ which affected J_{SC} is not governed by the temperature Eq. (8) [9]:

$$G(x) = -\mathrm{d}\Phi/\mathrm{d}x = \alpha_x \Phi(x_0)\exp(-\alpha_x x) \quad (8)$$

where, Φ is the flux density, α_x is the absorption constant, and the subscript x stands for layer.

Based on our model, when the temperature is below at 370 K, we always obtain a remaquable electrical parameters (V_{OC} = 0.5142, J_{SC} = 34.757, FF = 72.26, η = 12.91). In our case, the losses as a function of the temperature are estimated at 0.17%/K. According to Chelvanathan, et al. [3], the losses due to the temperature are estimated at 0.32%/K for CIGS solar cells, which is in agreement with our observations.

3.4 Series and Shunt Resistances

In this paragraph, the effects of series (R_S) and shunt resistance (R_{Sh}) on the electrical parameters are described. Fig. 5 shows the series and shunt resistances effects on the *J-V* characteristics.

From Fig. 5a, we notice that, the increasing of series resistance causes an important decrease of the short circuit current density and slight increases the open circuit voltage. The fill factor also shows a significant decrease as well as the conversion efficiency (Table 5). These results show that, the increase of R_S promotes bulk recombination.

As shown in Fig. 5b and Table 6, the open circuit

Table 4 Values of electrical parameters of CIGS cell as function of temperature.

T (K)	V_{OC} (V)	J_{SC} (mA/cm²)	FF (%)	η (%)
280	0.7085	34.628	79.1	19.4
300	0.6658	34.662	78.14	18.01
320	0.623	34.687	76.77	16.59
340	0.5799	34.711	75.11	15.12
360	0.5361	34.739	73.27	13.65
380	0.4922	34.778	71.18	12.18
400	0.4481	34.829	68.82	10.74

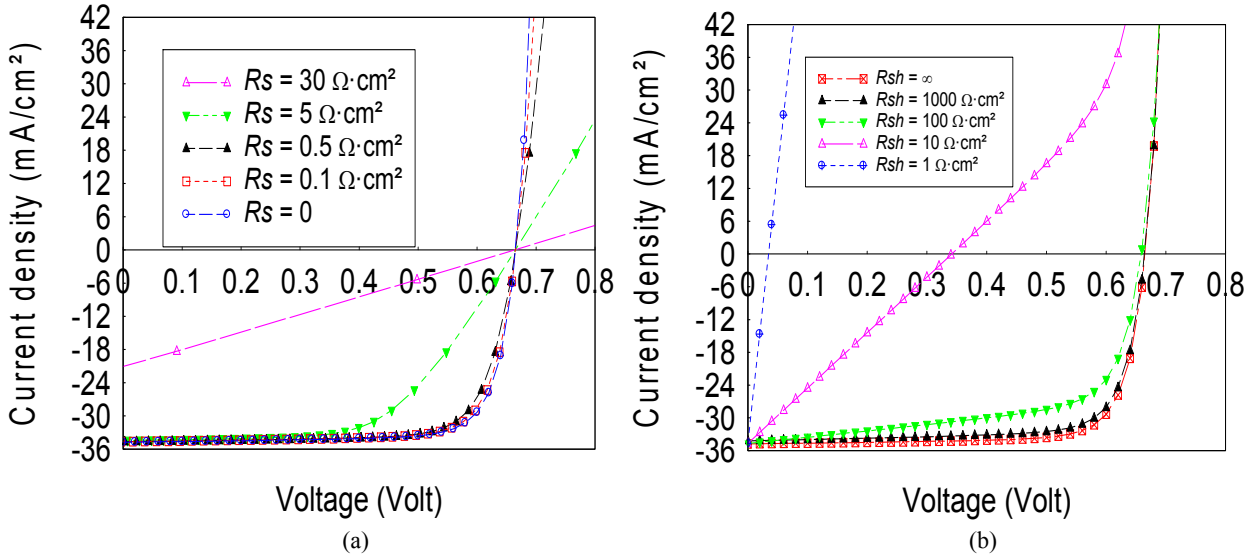

Fig. 5 *J-V* curves as a function of (a) R_S, (b) R_{Sh}.

Table 5 Electrical parameters as a function of R_S.

R_S (Ω·cm²)	V_{OC} (V)	J_{SC} (mA/cm²)	FF (%)	η (%)
0	0.6658	34.662	78.14	18.01
0.1	0.6659	34.658	77.71	17.94
0.5	0.6661	34.642	76.01	17.54
1	0.6663	34.62	73.89	17.05
5	0.6667	34.434	57.78	13.26
30	0.6668	21.15	27.31	3.85
60	0.6669	10.907	25.11	1.83

Table 6 Electrical parameters as a function of R_{Sh}.

R_{Sh} (Ω·cm²)	V_{OC} (V)	J_{SC} (mA/cm²)	FF (%)	η (%)
0.1	4.10^{-3}	34.662	-	-
1	0.034	34.662	25	0.3
10	0.341	34.662	25.1	2.96
10^2	0.658	34.662	65.1	14.87
10^3	0.665	34.662	76.8	17.71
10^4	0.665	34.662	78.0	18
10^{30}	0.665	34.662	78.1	18.04

voltage, fill factor and conversion efficiency decrease considerably at low values of shunt resistance due to the interface recombinations.

The combined effects of high R_S and low R_{Sh} decrease considerably the maximum-power point.

According to our results, the values of R_S in the range of 0.1-1 Ω·cm² and R_{Sh} superior to 1,000 Ω·cm² is ideal to achieve high performance.

To have an acceptable value of R_S and R_{Sh} near these value, we can dope the buffer layer high that the absorber layer. For our model, CIGS layer is doped at 7×10^{15} cm^{-2} and CdS layer is doped at 2×10^{17} cm^{-2} (Table 1).

4. Conclusions

Nowadays, numerical simulation of polycrystalline thin-film solar cells offers advantages to the design, performance prediction, and comprehension of the fundamental and complex phenomena. It is an important strategy to test the viability of proposed physical explanations and predict the effect of physical changes on cell performance.

In this paper, we have studied the influence of the CdS thickness, temperature, series resistance and shunt resistance on the performances of the hetero-structure Mo/CIGS/CdS/ZnO.

The simulated results show good performances when the thickness of the buffer layer is in the range of 10-40 nm due to the reduction of absorption in the short wavelenghts (380-500 nm). High performances of the model is obtained when the series and shunt resistances is in the range of 0.1-1 Ω·cm² and 1,000 Ω·cm², respectively. Under these conditions, the solar cells can operate under an ambiant temperature of 370 K without any losses of its performances.

Acknowledgments

The author gratefully acknowledges the use of SCAPS-1D developed by Marc Burgelman and colleagues at the University of Gent.

We also acknowledge the project PIMASO, a program financed by the European Union for financing the mobility of Daouda OUBDA at the University of Yaounde I.

References

[1] Chia-Hua, H. 2008. "Effects of Junction Parameters on $Cu(In,Ga)Se_2$ Solar Cells." *Journal of Physics and Chemistry of Solids* 69 (2-3): 779-83.

[2] Jackson, P., Dimitrios, H., Roland, W., Wiltraud, W., and Michael, P. 2014. "Compositional Investigation of Potassium Doped $Cu(In,Ga)Se_2$ Solar Cells with Efficiencies up to 20.8%." *Phys. Status Solidi RRL* 8 (3): 219-22.

[3] Chelvanathan, P., Mohammad, I. H., and Nowshad, A. 2010. "Performance Analysis of Copper-Indium-Gallium-Diselenide (CIGS) Solar Cells with Various Buffer Layers by SCAPS." *Current Applied Physics* 10 (3): S387-S391.

[4] Nakada, T., and Kunioka, A. 1999. "Direct Evidence of Cd Diffusion into $Cu(In,Ga)Se_2$ Thin Films during Chemical-Bath Deposition Process of CdS Films." *J. Applied Physics Letters* 74 (17): 2444.

[5] Tanaka, K., Takashi, M., and Hideyuki, T. 2009. "Analysis of Heterointerface Recombination by $Zn_{1-x}Mg_xO$ for Window Layer of $Cu(In,Ga)Se_2$ Solar Cells." *Solar Energy* 83 (4): 477-9.

[6] Cernivec, G., Krc, J., Smole, F., and Topic, M. 2006. "Band-Gap Engineering in CIGS Solar Cells Using Nelder-Mead Simplex Optimization Algorithm." *Thin Solid Films* 511-512 (July): 60-5.

[7] Marc, B., Alex, N., and Sofie, G. 1998. "SCAPS-1D User Manual Version 2.0." ELIS (Electronics and Information Systems), University of Gent Pietersnieuwtraast.

[8] Niemegeers, A., Marc, B., Stefaan, D., Johan, V., and Koen, D. 2012. "SCAPS Manual Version 24." ELIS, University of Gent Pietersnieuwtraast.

[9] Gloeckler, M. 2005. "Device Physics of $Cu(In,Ga)Se_2$ Thin-Film Solar Cell." Doctoral thesis, Colorado State University.

[10] Ana, K. 2007. "Anticipated Performance of $Cu(In,Ga)Se_2$ Solar Cells in the Thin-Film Limit." Doctoral thesis, Colorado State University.

[11] Kronik, L., David, C., and Hans, W. S. 1998. "Effects of Sodium on Polycrystalline $Cu(In,Ga)Se_2$ and Its Solar Cell Performance." *J. Advanced Materials* 10 (1): 31-6.

[12] Caballero, R. 2009. "The Influence of Na on Low Temperature Growth of CIGS Thin Film Solar Cells on Polyimide Substrates." *Thin Solid Films* 517 (7): 2187-90.

[13] Platzer-Björkman, C. 2006. "Band Alignment between ZnO-Based and $Cu(In,Ga)Se_2$ Thin Films for High Efficiency, Solar Cells." Doctoral thesis, Universitatis Upsaliensis Uppsala.

[14] Ouédraogo, S., Zougmoré, F., and Ndjaka, J. M. 2013. "Numerical Analysis of Copper-Indium-Gallium-Diselinide-Based Solar Cells by SCAPS-1D." *International Journal of Photoenergy* 2013 (2): 1-9. Accessed August 7, 2013. http://dx.doi.org/10.1155/2013/421076.

[15] Movla, H. 2014. "Optimization of the CIGS Based Thin Film Solar Cells: Numerical Simulation and Analysis." *Optik* 125 (1): 67-70.

[16] Niemegeers, A., Sofie, G., and Marc, B. 1998. "A Use Program for Realistic Simulation of Polycrystalline Heterojunction Solar Cells: SCAPS-1D." In *Proceedings of the 2nd World Conference on Photovoltaic Energy Conversion,* 672-5.

[17] Decock, K., and Burgelman, M. 2010. "SCAPS 3.0.01.2010." University of Gent Dept. Electronics and Info. St-Pietersnieuwstraat 41 B-9000 Gent, Belgium.

[18] Lide, D. 1991. *Hand Book of Chemistry and Physics.* Paris: Dunod , 91-2.

[19] Gloeckler, M., Fahrenbruch, A. L., and Sites, J. R. 2003. "Numerical Modeling of CIGS and CdTe Solar Cells: Setting the Baseline." In *Proceedings of the 3rd World Conference on Photovoltaic Energy Conversion,* 491-4.

[20] Burgelman, M. 2007. "Numerical Simulation of Thin Film Solar Cells, Practical Exercises with SCAPS." In *Proceedings of the NUMOS (Int. Workshop on Numerical Modelling of Thin Film Solar Cells),* 357-66.

[21] Benmir, A., and Aida, M. S. 2013. "Analytical Modeling and Simulation of CIGS Solar Cells, Terra Green 13 International Conference, Advancements in Renewable Energy and Clean Environment." *Energy Procedia* 36 (August): 618-27.

[22] Eisenbarth, T. 2010. "Interpretation of Admittance, Capacitance-Voltage, and Current-Voltage Signatures in $Cu(In,Ga)Se_2$ Thin Film Solar Cells." *J. Appl. Phys.* 107 (3): 034509. doi:10.1063/1.3277043.